Journal of Power Sources 216 (2012) 179–186

Contents lists available at SciVerse ScienceDirect

Journal of Power Sources

journal homepage: www.elsevier.com/locate/jpowsour

Surface studies of high voltage lithium rich composition: $Li_{1.2}Mn_{0.525}Ni_{0.175}Co_{0.1}O_2$

Surendra K. Martha, Jagjit Nanda*, Gabriel M. Veith, Nancy J. Dudney

Materials Science and Technology Division, Oak Ridge National Laboratory, Oak Ridge, TN 37831, USA

HIGHLIGHTS

- High voltage cycling (4.9 V) of lithium rich $Li_{1.2}Mn_{0.525}Ni_{0.175}Co_{0.1}O_2$ cathode.
- Surface film formation because of the oxidation of electrolyte.
- Studies of surface film using EIS, XPS and micro-Raman spectroscopy.
- Increase in cell impedance due to formation of polycarbonates, LiF, Li_xPF_y etc.
- Formation of thick surface film is the dominant reason for decrease in capacity.

ARTICLE INFO

Article history:
Received 15 March 2012
Received in revised form
17 May 2012
Accepted 18 May 2012
Available online 27 May 2012

Keywords:
Lithium battery
Li-rich MNC
Impedance
Surface chemistry
XPS
Micro-Raman spectroscopy

ABSTRACT

This article reports the evidence of surface film formation due to the oxidation of electrolyte upon high voltage cycling (4.9 V) of the lithium rich cathode, $Li_{1.2}Mn_{0.525}Ni_{0.175}Co_{0.1}O_2$. We have studied the chemical composition of this surface film using electrochemical impedance, X-ray Photoelectron and micro-Raman spectroscopies and the results are compared against the pristine electrode. In order to distinguish the changes in the surface film composition induced by prolonged electrochemical cycling versus chemical passivation effect, we studied the surface composition of cathode powders aged with electrolytes at 60 °C. Our results show that after 150 cycles, the electrodes showed a rapid drop in capacity due to increase in the surface film resistance resulting in limited capacity utilization.

1. Introduction

In a recent article [1] we reported the electrochemical performance of the lithium rich cathode material, $Li_{1.2}Mn_{0.525}Ni_{0.175}Co_{0.1}O_2$ (hereafter called Li-rich MNC) or alternatively written in the layered–layered notation as $0.6Li[Li_{1/3}Mn_{2/3}]O_2–0.4Li[Mn_{0.3}Ni_{0.45}Co_{0.25}]O_2$. We demonstrated an improvement in rate capability and cycling performance with the addition of 1.5 wt. % of highly graphitic carbon nanofiber (CNF) to the electrode composition. The capacity of the Li-rich MNC electrodes, without CNF, falls rapidly after 120–150 cycles; however, Li-rich MNC electrodes with CNF maintain a steady capacity for more than 200 cycles [1]. The origin of this enhanced cycling performance could be because the CNFs help to maintain a good electronic network around the Li-rich MNC particles enabling electron transport through the insulating surface film formed because of high voltage cycling. It is known that the surface structure and composition of the active material, and their reactivity with electrolyte under electrochemical cycling, play an important role in determining their electrochemical performance and cycle life [2–8]. These aspects are even more important at higher cycling voltages (up to 5 V), since all standard electrolyte mixtures are unstable at voltages >4.4 V and therefore prone to form oxidation products on the surface [2–7,9–14]. In addition, repeated electrochemical cycling at higher voltages lead to multiple transition metal cations (Mn, Ni, Co) species migration to the surface and react with electrolyte forming various reaction products on the surface [2–7,9–13]. Alternatively, the transition metal cations can also dissolve in the electrolyte solution and potentially migrate to the negative electrode [15–18]. All these processes can lead to capacity fade as well as contribute to the overall increase in cell impedance leading to power fade. Surface chemistry therefore, plays a major factor in determining the long-term stability and cycle life of lithium-ion cells since a majority of the current cells use lithium transition metal oxide as their positive electrodes [2–12]. Methods such as electrochemical impedance spectroscopy (EIS)

* Corresponding author. Tel.: +1 865 2418361; fax: +1 865 5746210.
E-mail address: nandaj@ornl.gov (J. Nanda).

0378-7753/$ – see front matter © 2012 Elsevier B.V. All rights reserved.
doi:10.1016/j.jpowsour.2012.05.049

have identified the formation of surface films on lithium transition metal oxide based cathodes as the source of increase in cell impedance and decrease in cycle efficiency [19,20]. The Li^+ ions must also travel through an additional interphase layer between cathode and electrolyte: a process that could be rate limiting if the surface species formed on top of cathode surface are poor Li-ion conductors and insulating with respect to electronic conduction. This study reports the surface composition and chemistry of high voltage Li-rich MNC cathodes when subjected to high voltage electrochemical cycling (up to 4.9 V) and the results are correlated with observation from EIS studies.

Further, we performed a comparative study of the nature of the surface film composition between cycled, pristine cathode and Li-rich MNC powder aged with electrolyte versus pristine powder using X-ray photoelectron spectroscopy (XPS) and micro-Raman analysis. The overall goal is to understand and identify the various capacity and rate limiting processes that could results the Li-rich positive materials were cycled in the region of unstable electrolyte stability region where the surface reactivity and oxidation reactions are dominant.

2. Experimental

2.1. Electrochemical measurements

Li-rich MNC powder was obtained from the pilot scale synthesis facility of TODA Materials Corporation, Japan and detailed structural and electrochemical characterization studies were performed at Oak Ridge National Laboratory [1]. The electrochemical performance of the cathodes comprising Li-rich MNC as the active mass were evaluated using two and three-electrode coin-type cells (size CR2032, Hohsen Corp. Japan) with a 25 μm microporous trilayer membrane (polypropylene/polyethylene/polypropylene) separator (type 2325, Celgard, Inc., USA). Electrodes for electrochemical evaluation were prepared with an *N*-methylpyrrolidone (NMP) (Aldrich, 99.5% purity) slurry of Li-rich MNC, polyvinylidene fluoride (PVDF) (Aldrich), and C-black (CB) (Super P) in wt. % ratio of 85:7.5:7.5. The slurry was coated on one side of the Al foil (Alfa Aesar, 99.99% purity) current collector with positive active material loading of 7–10 mg cm^{-2}. Lithium foils (purity 99.9%, Alfa Aesar) were used as counter and reference electrodes. The electrolyte solution was 1.2 M $LiPF_6$ in a 1:2 mixture of ethylene carbonate (EC) and dimethyl carbonate (DMC) by weight (battery grade, Novolyte Technologies, USA). Electrochemical cells were assembled in a glove box filled with high purity argon. After assembling, the cells were stored at room temperature for about 12 h to ensure complete impregnation of the electrodes and separators with the electrolyte solution.

Galvanostatic charge–discharge cycling was carried out using a multichannel battery tester (model 4000, Maccor Inc., Tulsa, OK, USA) in two-electrode coin-type cells. Cells were cycled in a potential range of 2.5–4.9 V using a constant current plus constant voltage (CC–CV) charge, i.e. charging continued at 4.9 V until the current reached a value corresponding to C/50 value. Discharge tests were performed using constant current protocol at various rates to the 2.5 V cut-off potential.

EIS measurements of Li-rich MNC composite electrode were carried out during the 1st, 50th and 200th delithiation cycle using a battery test unit model 1470E coupled with a frequency response analyzer model 1455 from Solartron Analytical Ltd., controlled by ZPlot software from Scribner Associates. EIS studies were carried out in 3-electrode configurations using lithium metals as counter and reference electrode. For the EIS measurements, the electrode potential was increased stepwise from 3.0 V (open circuit voltage) to 4.9 V with 0.1–0.2 V potentiostatic steps. The current was monitored for 2 or 3 h to observe the relaxation to a steady state current value <5 μA cm^{-2}. Following equilibration at each potential, EIS was carried out from high frequency 1 MHz to low frequency 5 mHz with 10 points per decade in frequency and amplitude of 10 mV. For clarity, only few relevant voltages are presented in the figures. EIS are normalized by the geometric area ($\sim$1 cm^2) of the electrode.

2.2. Surface characterization

The surface chemistry of the Li-rich MNC powders (no binder or carbon black) in contact with the electrolyte solutions was tested by soaking at 60 °C for 10 days. This was carried out in an argon-filled glove box using magnetic stirrers with 1.5 g of powder in $\sim$7 ml of standard EC-DMC 1:2/$LiPF_6$ 1.2 M solution. Before characterization, the materials (hereafter-aged powders) were separated from solution by centrifugation, washed several times with anhydrous DMC solvent and dried under vacuum for 12 h. Electrodes, both pristine and fully delithiated (4.9 V) cathodes after 200 cycles, as well as Li-rich MNC powders, pristine and aged, were characterized using a PHI 3056 X-ray photoelectron spectrometer with an Al anode source operated at 15 kV and an applied power of 350 W. For surface analysis, the cycled cells were disassembled in an argon-filled glove box, washed with anhydrous DMC, dried under vacuum for overnight and transferred via a load locked system to the XPS chamber to avoid air exposure. High resolution scans were taken with 23.5 eV pass energy, 0.05 eV energy step, and from 50 to 100 repeats to improve the signal to noise ratio. Survey scans were measured at 93.9 eV pass energy, 0.5 eV energy step and 25 repeats. The binding energies are shifted by setting the aliphatic carbon signal to 284.8 eV. The spectra were deconvoluted using Gaussian–Lorentzian functions based on PHI MultiPak software.

Raman spectroscopy of these cathodes (pristine and fully delithiated (4.9 V) cycled) and powders (pristine and aged) was carried out using an Alpha 300 confocal micro-Raman setup manufactured by WITec Inc., Germany. Raman microscopy measurements were performed using a solid-state 532 nm excitation laser with a 20X objective and 600 g mm^{-1} (grooves per millimeter) grating. Samples for *ex situ* Raman measurements were prepared with pristine and cycled electrodes; and pristine and aged powders sandwiched between two thin glass cover slides (0.15 mm thickness) and sealed under argon atmosphere using ultra-high vacuum glue. XPS and Raman studies were carried under fully delithiation stage by charging the electrodes up to 4.9 V using above CC–CV charging protocol until the current reached to a corresponding C/200 value in the potentiostatic step. Similar charging protocol was used for the Li-rich MNC electrode maintained at 4.5 V. For Raman studies, representative spectra were collected at various locations of the electrode to ascertain reproducibility. Spectral deconvolution of the Raman peaks was performed using Lorentzian line profile based on Origin 8.1 software package.

3. Results and discussion

3.1. Surface morphology and electrochemical assessments

The details of structure and morphology of Li-rich MNC particles used in this study are reported in our earlier paper [1]. In short, the Li-rich MNC particles are spherical in shape with aggregated secondary particles of diameter ranging between 2 and 15 μm and primary particles with sizes between 80 and 110 nm (Fig. 1(a)). The active surface area of the material measured by BET method was about 3.2 m^2 g^{-1}. The tap density of material was about 1.74 g cm^{-3} as per the data provided by the materials supplier.

Fig. 1(b) presents cycling performance of Li-rich MNC composite electrodes for 250 cycles. Typically, the Li-rich MNC composite electrodes studied herein exhibit an initial stable discharge

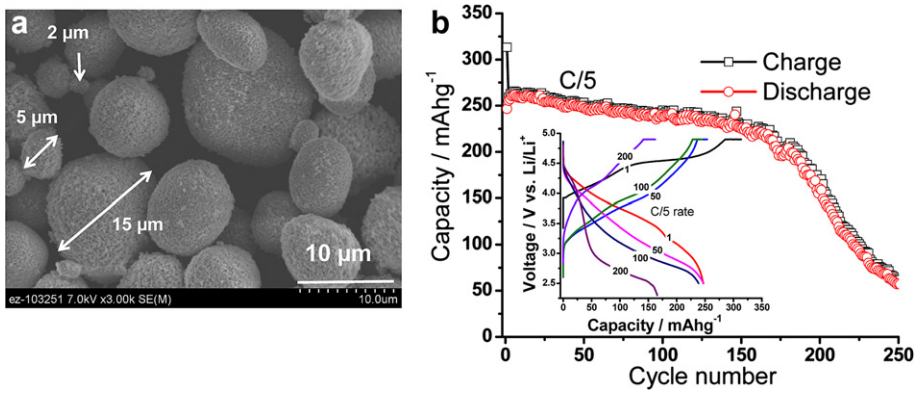

Fig. 1. (a) SEM image of bare Li-rich MNC particles (X 3000; scale bars are 10 μm). (b) Charge–discharge cycling datas of Li-rich MNC composite electrodes at C/5 rate in EC-DMC 1:2/$LiPF_6$ 1.2 M solutions (at 25 °C). Inset to Fig. 1(b): Corresponding voltage profiles for various cycles (numbers are indicated in the figure). Cycling protocol was constant current – constant voltage step at 4.9 V *vs.* Li/Li^+ until the current reach value of C/50. The lower cut off potential was 2.5 V *vs.* Li/Li^+till 100 cycle and 2.0 V *vs.* Li/Li^+ between 100 and 200th cycle.

capacity of ∼260 mAh $g^{-1}$of capacity at C/5 rate. The charge–discharge voltage profiles versus cycle number are presented in the inset to Fig. 1(b). With prolonged cycling the Li-rich MNC, composite electrodes have lost almost all of their original capacity. Further replacing the cycled Li-metal foil with a new one did not improve the capacity fade, which would indicate the loss of capacity is due to the cathode. Moreover, discharge profiles (inset to Fig. 1(b)) move to lower voltage plateaus showing significant loss of energy. The origin of such rapid drop in the discharge voltage profile is not fully understood at present but could be related to the gradual change to a spinel-like structure [21]. This data (Fig. 1(b)) clearly suggests that the limited capacity retention upon prolonged cycling in Li-rich MNC electrode could due to significant reduction in the electronic conductivity because of the formation of insulating electrolyte decomposition and reaction products, as discussed later with our XPS results. In contrast to these, our recent results on carbon nanofiber (CNF) added Li-rich MNC electrodes shows these electrodes maintain stable capacities for hundreds of cycles [1]. The CNFs provide an effective electronic wiring around the surface of the active material forming an interconnected conducting pathway across the bulk of the electrode despite the formation of a surface passivation films due to electrochemical cycling up to 4.9 V.

The formation of surface film on the surface of the positive active material affects the electrochemical processes occurring during the charge–discharge cycles. The passivation films protects the surface of the electrode particle by avoiding direct contact with electrolyte solution during the highly oxidizing charging environment but at the same time could increase the cell impedance affecting the cycling efficiency and capacity utilization. Monitoring the impedance spectra at different state of charge (SoC) as a function of electrochemical cycling can provide important information about the surface passivation film. In Fig. 2, we show the EIS, presented as Nyquist plots, of Li-rich MNC composite electrodes at 25 °C measured during (a) 1st cycle and (b) 50th and (c) 200th cycle at various equilibrium potentials: 3.0 V, 4.0 V, 4.5 V, and 4.9 V. The magnified images of the high frequency region of the EIS are shown in Fig. 2(d)–(f) and mid-frequency regions are shown in Fig. 2(g)–(i). As part of the EIS analysis, the general trend is to assign a time constant (RC) to each of the transport processes and analyze within an equivalent circuit model. However, the individual EIS features as shown are highly distorted making distinct RC analysis for each transport processes difficult. It plausible that the complex nature of the material system and associated surface film growth upon high voltage cycling have various transport process overlap in the Nyquist plot. Therefore, here we only provide a qualitative discussion of the EIS results.

Based on earlier work by Paasch et al. [22] on EIS of porous electrodes the first high frequency semicircle corresponds to the double layer charging associated with porous electrode originating from ionic resistance inside the pores followed by double layer capacitance associated with the active material surface. This feature should be voltage independent as clearly demonstrated in the data. The values of *R* in the 1st loop in the high frequency (1 MHz) domain down 6.3 kHz are 57, 95, 43 Ω cm^2 during 1st, 50th and 200th cycle. The magnified images in the mid-frequency regions of the Fig. 2(a)–(c) are presented in Fig. 2(g)–(i) showing the surface film growth with increasing cycle number.

We also notice (Fig. 2(d) and (f)) that as a result of prolonged cycling, the ohmic component of the complex impedance increases from 10 Ω cm^{-2} during the 1st cycle to 20 Ω cm^{-2} in the 200th cycle primarily due to increase in the electrolyte resistance. The mid-frequency loop in all three cases (1st, 50th and 200th) is associated with surface film primarily due to oxidation of electrolyte upon cycling. This feature clearly grows with successive cycling (magnified figures shown in Fig. 2(g)–(i)) to the extent that it becomes the rate limiting step for 200 cycle EIS data (Fig. 2(c)) completely dominating the transport process in the measured frequency range. The third frequency component for the analysis of the low frequency loop for 1st and 50 cycle EIS data is complicated as it involves both charge transfer, which can be SoC dependent, and finite solid state diffusion effect. As mentioned earlier, for porous electrode like Li-rich MNC with wide range particle size distribution (in this case between 2 and 15 microns, Fig. 1(a)) and uneven active materials distribution across electrode thickness, the finite diffusion region at lower frequency can have a distorted shapes [23–25].

3.1.1. *X-ray photoelectron spectroscopy (XPS) of cycled cathodes*

Along with EIS study at different SoCs, XPS of charged as well as pristine electrodes were carried out to determine the chemical composition of passivation products formed as results of high voltage cycling. Two kinds of processes are expected to occur upon high voltage cycling, (i) surface species formation due to oxidation of electrolyte (ii) selective diffusion of transition metal cations to the surface driven by repeated lithiation (delithiation). However, given the limited surface sensitivity of the XPS, the electrolyte oxidation products layer may screen some of the transition metal signal from surface of the Li-rich MNC particle. Fig. 3 presents XPS spectra of (a) P2p, (b) C1s, (c) O1s, (d) F1s, (e) Mn2p, (f) Ni2p3/2, and (g) Co2p3/2 of pristine and cycled cathodes (fully delithiated cathode at 4.9 V after 200 cycles). The pristine cathode has no electrolyte oxidation product hence no phosphorus XPS signal. In contrast, the cycled electrodes exhibits a broad P2p signal (Fig. 3(a))

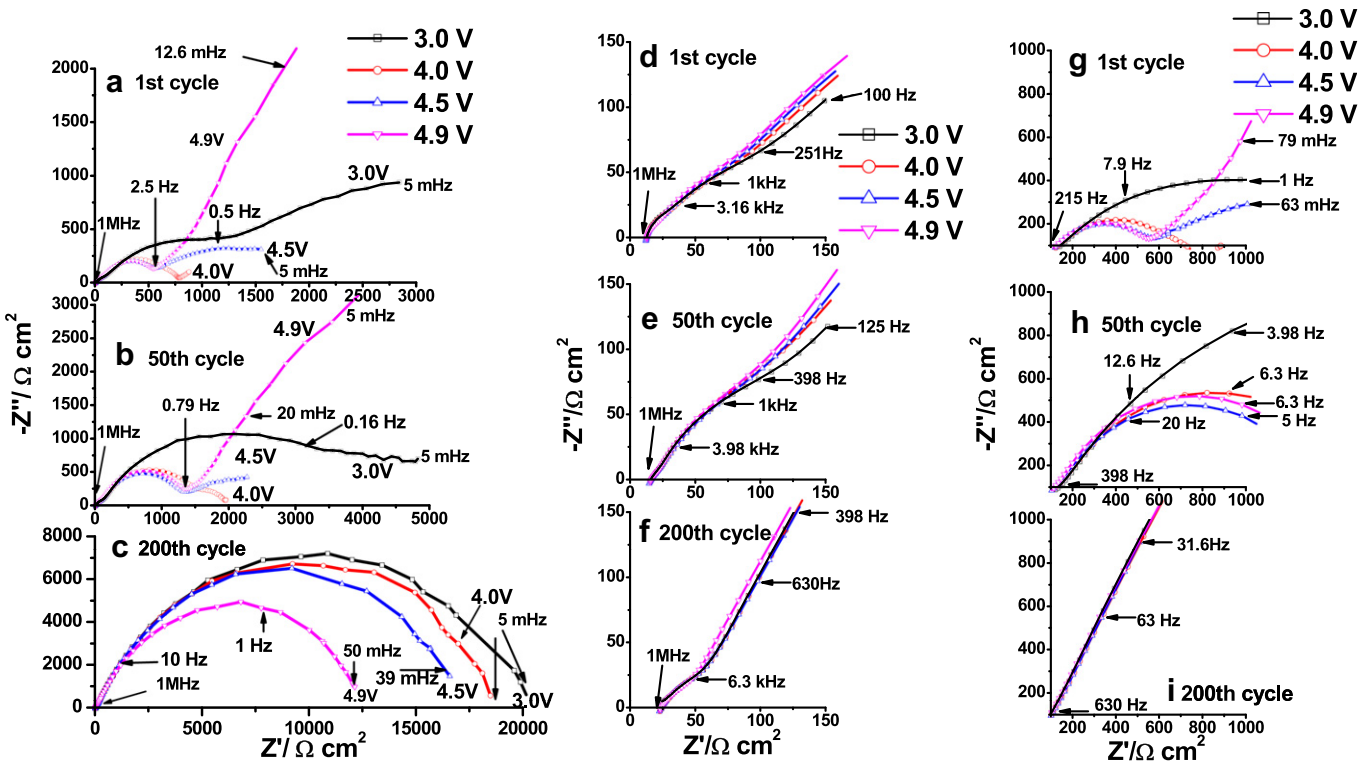

Fig. 2. A family of impedance spectra, represented as Nyquist plots, of Li-rich MNC composite electrodes at 25 °C measured during (a) 1st cycle, (b) 50th cycle and (c) 200th cycle between the frequency range 1 MHz and 5 mHz. Zoomed images of high to medium frequency (1 MHz–~100 Hz) semicircle are shown during (d) 1st cycle, (e) 50th cycle and (f) 200th cycle; and med-frequency (~100–1 Hz) regions are shown during (g) 1st cycle (h) 50th cycle and (i) 200th cycle at various equilibrium potentials 3.0 V, 4.0 V, 4.5 V, and 4.9 V, as indicated at T=25 °C during Li-deintercalation processes.

resulting from the oxidation of the $LiPF_6$ salt corresponding to a Li_xPF_y component at close to 136 eV and $Li_xPF_yO_z$ type compound at a lower binding energy (BE), 134 eV [2,7,9,26].

The C1s spectra in Fig. 3(b) in the pristine sample have three significant components. The higher binding energy component around 291 and 286 eVs corresponds to the binder PVDF and can be assigned to C–F, C–C, C–O, C=O and C–H type chemical environment and the lower BE peak at 285 eV corresponds to the carbon from the carbon diluents [2,7,10,11,26].

Upon cycling, the C1s peak in cycled fully delithiated cathodes shows formation of significant polycarbonates, $ROCO_2Li$ (CO_3^{2-}) (R represents alkyl group) species, with binding energies at 289 and 286 (C–O). The, C–F chemical environment of binder PVDF at 291 eV is invisible in the fully delithiated cycled cathodes and is therefore likely buried beneath the surface film that forms. Another peak at 284.5 eV corresponds to amorphous carbon C1s signal. The results from carbon core level signals appears to be consistent with O1s core level result for pristine and cycled electrodes shown in Fig. 3 (panel c). The pristine electrode has a layer of organic C–O type species on the surface represented by a broad peak at 533 eV and the lattice oxygen signal at 530.3 eV. The binding energy feature at 533 eV may also from the hydroxyl (OH) species, which could originate from metal hydroxide residue from the synthesis, or from a reaction with moisture in the air. The lattice oxygen part is completely suppressed (only a weak feature at 529.6 eV) in case of cycled cathodes due to the thick electrolyte oxidation layer showing primarily the carbonate (lithium) species at 532.5 eV [2,3,6–10,15,26,27].

The F1s spectrum (Fig. 3(d)) of pristine cathodes predominantly shows a single BE feature at 688.6 eV corresponding to the characteristic C–F species of the binder PVDF. This feature is markedly absent in cycled electrodes due to the formation of the thick surface film layer described previously. Instead, there is a new F1s peak at 687.5 eV due to the formation of P–O–F, P–F type compositions. The strong XPS signal close to 685 eV for cycled electrode is due to the formation LiF compounds [2,5,7,10]. The formation of LiF and PF_5 (P–F bonded compound) could be due to the oxidation of $LiPF_6$ at high operating voltage (4.9 V). Alternatively the F1s species could be due to the reaction of surface oxygens (Li_2O) with acidic species such as HF from the electrolyte or reaction with surface OH's as evidenced in the O1s data (Fig. 3(c)). LiF formed on the surface may react with traces of HF in the electrolyte can form PF_3O (P–O–F bonded compounds).

The transition metal XPS core levels (Fig. 3(e)–(g)) of both pristine and cycled electrodes were monitored to examine their relative surface composition as they undergo repeated electrochemical cycling to higher voltages. In the cycled electrodes, there was a significant reduction in the Mn and Ni signals and complete loss of Co species. For cycled cathode, we notice a very broad feature in Ni2p data, could be attributed to F (KL, L_{23}) auger line, which overlaps with the Ni2p spectra. In any case it is clear that the metal signals are reduced or eliminated due to the thick surface layer (LiF, etc.) that forms with cycling which must be >5 nm thick to attenuate the 3d metal photoelectrons.

3.1.2. XPS of electrolyte-aged powders

Fig. 4 compares (a) C1s, (b) O1s, (c) P2p, (d) F1s, (e) Mn2p, (f) Ni2p3/2, and (g) Co2p3/2 XPS spectra of pristine and electrolyte-aged Li-rich MNC powder (no PVDF and CB) in EC-DMC/$LiPF_6$ solution. There are no significant changes between the XPS spectra of Ni, Mn, Co (Fig. 4(e)–(g)) for the pristine and aged Li-rich MNC powder indicating no change in metal oxidation state.

The C1s spectra for the pristine powder in Fig. 4(a) show two significant peaks around 289 and 285 eV. The 285 eV peak could be attributed to residual carbon from the synthesis and contaminants present in the analysis chamber. The higher BE peak ~289 eV is be

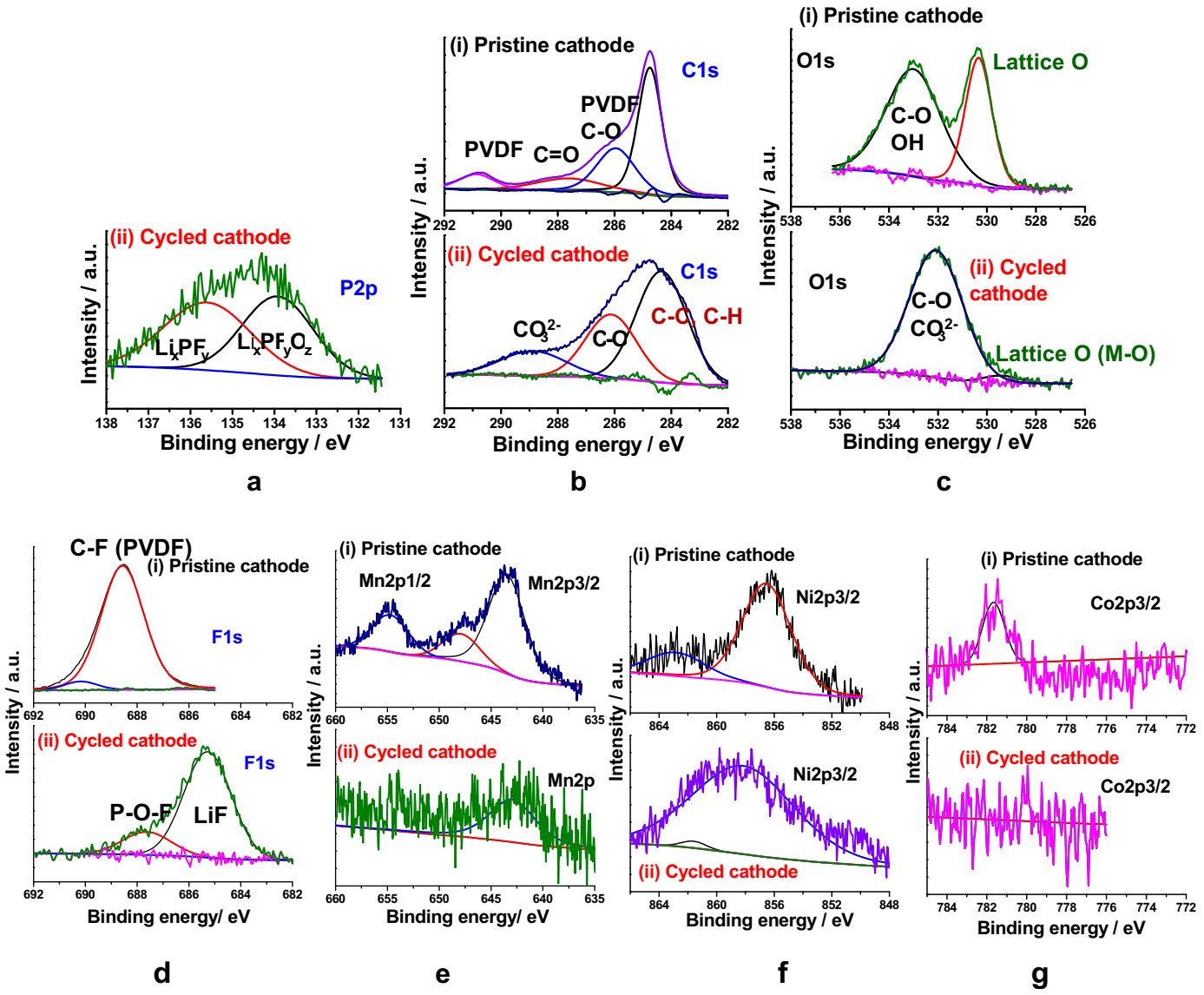

Fig. 3. XPS spectra for (a) P2p, (b) C1s, (c) O1s, (d) F1s, (e) Mn2p, (f) Ni2p3/2, and (g) Co2p3/2 measured from Li-rich MNC cathodes (i) pristine, (ii) fully delithiated (at 4.9 V) after 200 cycles at 25 °C in EC-DMC 1:2/$LiPF_6$ 1.2 M solutions.

ascribed to the formation of Li_2CO_3 surface impurity, which could be a residue from the synthesis precursors, or a product of reactions between CO_2 in the atmosphere and the active cathode powder [28]. Therefore, a Li_2CO_3 surface film on the electrode surface already exists in its pristine form. However, the pristine cathodes do not show Li_2CO_3 surface impurity at ~289 eV, because Li_2CO_3 might have covered beneath of the binder and conductive diluents in pristine cathodes or dissolved during processing.

The O1s spectra in Fig. 4(b) show significant changes between the aged and pristine Li-rich MNC powder. Similar to the cathodes, there is a strong O1s peak at 529.6 eV, which corresponds to lattice oxygen of Li-rich MNC, and a broad peak due to OH or metal carbonates (CO_3^{2-}) at 532.5 eV. The O1s spectra of aged powder show another distinct peak at 531.2 eV, which correspond to the organic ether linkages (C—O) [5,10,27,29]. Examination of C1s region spectra of the aged powder shows three distinct components at 285, 287 and 289 eV (small peak) which is consistent with O1s spectra is likely due to the presence of carbon (C—C), ethers (C—O) and carbonates (CO_3^{2-}, lithium alkyl carbonates, polycarbonates), respectively. The ether linkage in C1s and O1s spectra is likely due to the presence of poly (ethylene oxide) on the surface of aged Li-rich MNC cathodes. As 289 eV C1s signal is very small, indicating the CO_3^{2-} was likely dissolved in the carbonate based electrolyte.

The P2p (Fig. 4(c)) peak at 135 eV arises from P atom that is bound to a less electronegative element than F. Formation of P_2O_5 or P—O—F bonded compounds have been suggested to form on the surface of lithium transition metal oxides upon aging at elevated temperatures [2,3]. There is a probability of presence of $Li_xPF_yO_z$-type compound, such as Li_2PFO_3, which originates from the hydrolysis of $LiPF_6$ [2]. This hydrolysis could occur via residual moisture or the OH evidenced in the XPS data. The fluorine spectrum (Fig. 4(d)) with a broad XPS peak at 687.5 eV reflects the formation of P—F bonded compounds such as $LiPF_6$ or related Li_xPF_y compounds, which were also observed in the P2p spectrum. Another distinct peak around 685 eV for aged F1s spectrum reflects formation of fluorine compounds such as LiF. This could be due to the slow reaction of Li_2CO_3 with acidic species, such as HF, which form surface fluorides (LiF), CO_2 and H_2O.

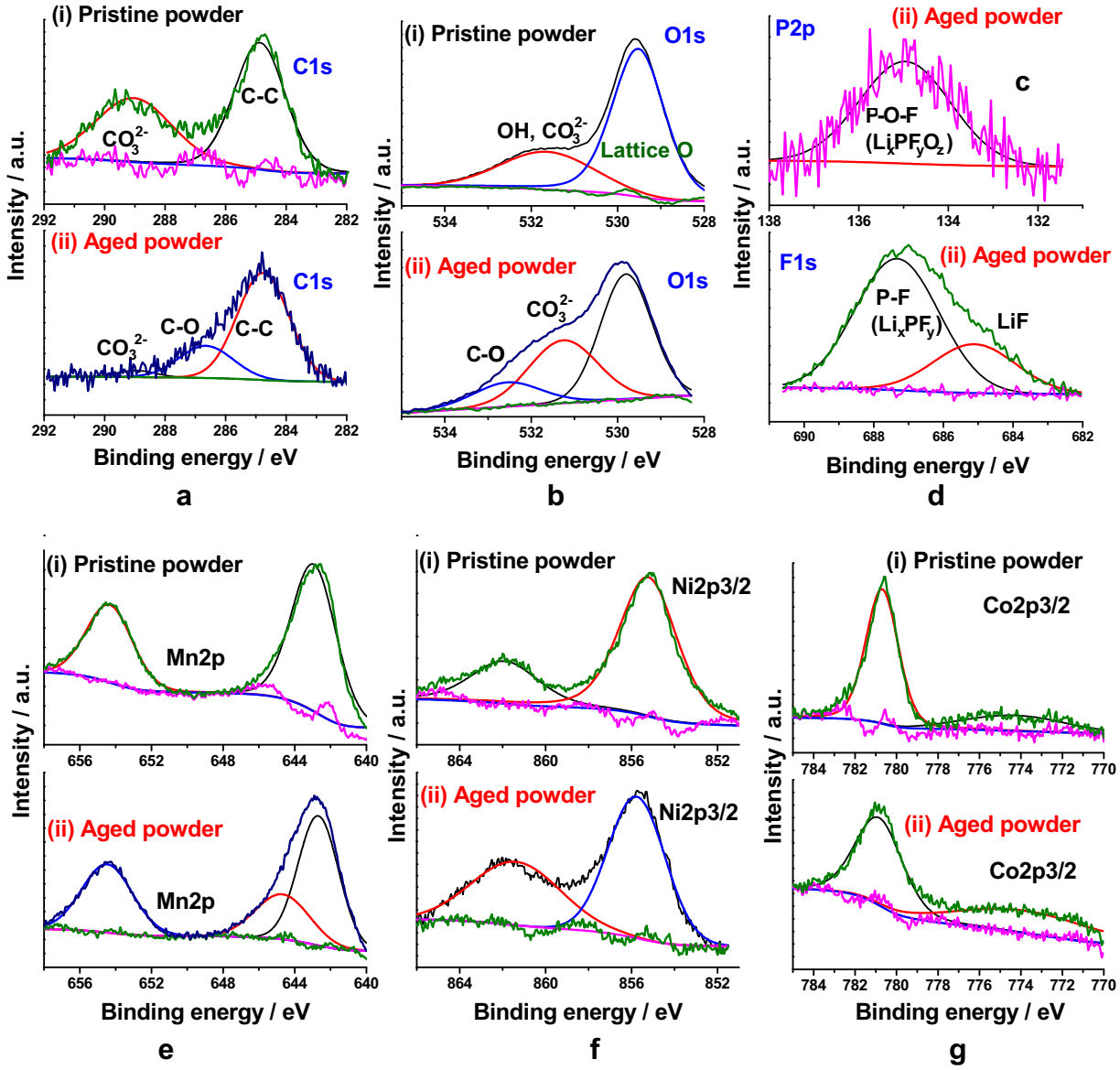

Fig. 4. XPS spectra for (a) C1s, (b) O1s, (c) P2p, (d) F1s, (e) Mn2p, (f) Ni2p3/2, and (g) Co2p3/2 measured from Li-rich MNC powders (i) pristine, (ii) aged during 10 days at 60 °C in EC-DMC 1:2/$LiPF_6$ 1.2 M solutions. These pristine and electrolyte-aged powders are free from binder (PVDF) and conductive additives (CB).

This clearly signifies that the Li-rich MNC compounds forms surface films, on treatment with electrolyte at elevated temperature, which is consistent with the observations for all other transition metal oxide cathodes reported in the literature [2,3,6–10,17,27,29].

3.2. Raman spectroscopy of cycled cathodes and electrolyte aged powders

Raman spectroscopy is a powerful method for probing the chemical nature of the electrochemical interface in a Li-ion battery [30]. Fig. 5(a) presents Raman spectra for pristine, delithiated to 4.5 V during first cycle and fully delithiated (4.9 V) Li-rich MNC cathodes after 200 cycles. The amorphous carbon used as conductive filler for the electrodes has the usual Raman D band around 1350 and a broad G band between 1590 and 1600 cm^{-1} both for pristine and charged electrodes. The total carbon signal was deconvoluted using four components to take into account of various disorder carbons and the graphitic form [31]. Pristine Li-rich MNC electrode show metal-oxygen (M – O) vibrations centered at 485 and 600 cm^{-1} corresponding to the in plane (E_g) and transverse (A_{1g}) oxygen vibrations, respectively. There is a weak peak at 419 cm^{-1} corresponding to the monoclinic Li_2MnO_3 phase [32]. When the electrodes are charged to 4.5 V and 4.9 V (Fig. 5(a), middle and bottom), the Li_2MnO_3 feature at ~419 cm^{-1} is no longer evident as expected. Further, the E_g and A_{1g} oxygen vibrations are shifted to 522 and 632 cm^{-1} and appear narrow (Fig. 5(a), bottom). By charging the electrodes up to 4.5 V during first cycle (Fig. 5(a), middle), the E_g and A_{1g} oxygen vibrations appears to be red shifted to 553 (broad peak) and 637 cm^{-1} (weak peak). Upon complete delithiation, both E_g and A_{1g} bands appear narrow and centered around 522 and 632 cm^{-1} respectively. Additionally, the integral peak intensity ratio between E_g and A_{1g} significantly changes from the pristine electrode to completely delithiated state, which is a spectroscopic signature of the local lithium concentration [32,33]. The sharpening of Raman band is associated with the decrease in the lattice disorder created by absence of lithium atoms in the interstitial layers during the delithiated or charged state [30].

Fig. 5(b) presents Raman spectra for pristine and chemically aged Li-rich MNC powders. The pristine powders have oxygen E_g

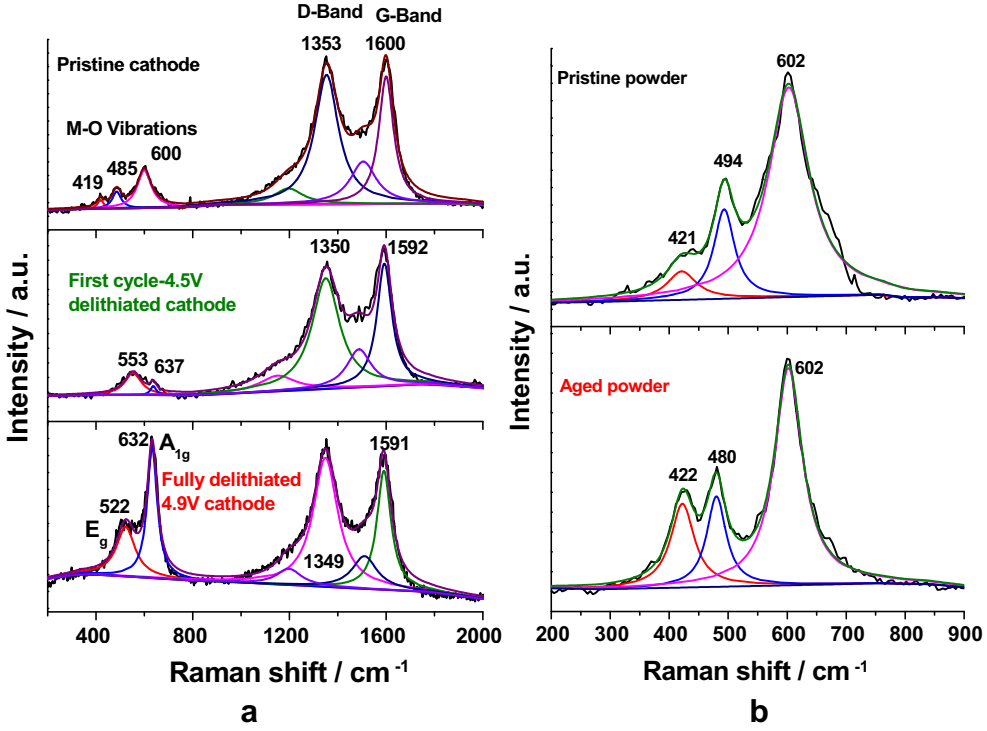

Fig. 5. Raman spectra for (a) pristine cathode, delithiated (4.5 V) cathode during 1st cycle and fully delithiated cathode (4.9 V) after 200 cycles for the composite Li-rich MNC cathode (as indicated), (b) pristine and electrolyte-aged Li-rich MNC powder (no PVDF and CB).

and A_{1g} components at 494 and 602 cm^{-1}, and the monoclinic Li_2MnO_3 peak at 422 cm^{-1}. Chemically aging the Li-rich MNC powders in electrolyte solution at elevated temperature have only a marginal effect on the Raman band as shown in Fig. 5(b) (bottom) with signatures of both Li_2MnO_3 and metal-oxygen. It is not clear at present why there is a large (14 cm^{-1}) difference in the E_g position between the pristine and the chemically aged powders. This shift could be due to strains associated with processing, and other chemical induced changes. Studies are underway to characterize the Li-rich MNC electrodes at various SoC using both *in situ* and *ex situ* micro-Raman spectroscopy.

4. Conclusions

Li-rich MNC electrodes have the limited capacity retention upon prolonged high voltage (4.9 V) cycling, due to significant reduction in the electronic conductivity because of the formation of insulating electrolyte decomposition and reaction products. EIS were monitored at different delithiation voltages as a function of electrochemical cycling which provides important information about the surface passivation film. The electrode impedance increases with increase in cycling affecting the cycling efficiency and capacity utilization. XPS and Raman studies were performed to study the nature of the surface passivation films and the compositional changes associated between pristine and delithiated powders and electrodes. The surface of the pristine Li-rich MNC particles contain Li_2CO_3, and hydroxides (−OH), which are residues from the synthesis precursors, or a product of reactions between CO_2 and moisture from the atmosphere and the active Li-rich MNC powder. Li-rich MNC compounds upon aging or cycling in electrolyte solutions containing alkyl carbonates can form $ROCO_2Li$, $(ROCO_2)_y$ M, ROLi and $(RO)_x$ M surface species. Li_2CO_3 with acidic species such as HF forms surface fluorides (LiF), CO_2 and H_2O. In cathodes, the surface oxygens react with acidic species such as HF and forms surface fluorides (LiF). Besides LiF, the surface films formed here are found to consist of salt-based products such as Li_xPF_y and $Li_xPO_yF_z$. EC may polymerize on Li-rich MNC particles forming polycarbonate species. Formation of surface films such as polycarbonates, LiF, Li_xPF_y and $Li_xPO_yF_z$ (as mentioned above) can cause increase in cell impedance during cycling as shown by our EIS study. Formation of surface film on Li-rich MNC particles because of high voltage cycling could be the dominant reason for decrease in capacity as shown in Fig. 1(b).

Acknowledgments

Materials used in this study were supplied courtesy of Toda Materials Corporation, Japan, lithium rich $Li_{1.2}Mn_{0.525}Ni_{0.175}Co_{0.1}O_2$. We thank Dr. Frank Delnick for technical discussion and valuable inputs for analysis of electrochemical impedance results. This work is supported by the Assistant Secretary for Energy Efficiency and Renewable Energy, Office of Vehicle Technologies of the U.S. Department of Energy. GMV acknowledges support from the Office of Basic Energy Sciences, Materials Sciences and Engineering Division, U.S. Department of Energy.

References

[1] S.K. Martha, J. Nanda, G.M. Veith, N.J. Dudney, J. Power Sources 199 (2012) 220–226.
[2] A.M. Andersson, D.P. Abraham, R. Haasch, S. MacLaren, J. Liu, K. Amine, J. Electrochem. Soc. 149 (2002) A1358–A1369.
[3] D. Aurbach, B. Markovsky, G. Salitra, E. Markevich, Y. Talyossef, M. Koltypin, L. Nazar, B. Ellis, D. Kovacheva, J. Power Sources 165 (2007) 491–499.
[4] D. Aurbach, Y. Talyosef, B. Markovsky, E. Markevich, E. Zinigrad, L. Asraf, J.S. Gnanaraj, H.-J. Kim, Electrochim. Acta 50 (2004) 247–254.
[5] D. Aurbach, J. Power Sources 89 (2000) 206–218.
[6] T. Eriksson, T. Gustafsson, J.O. Thomas, Electrochem. Solid State Lett. 5 (2002) A35–A38.
[7] L. Yang, B. Ravdel, B.L. Lucht, Electrochem. Solid State Lett. 13 (2010) A95–A97.
[8] Y. Talyosef, B. Markovsky, G. Salitra, D. Aurbach, H.J. Kim, S. Choi, J. Power Sources 146 (2005) 664–669.
[9] D. Aurbach, K. Gamolsky, B. Markovsky, G. Salitra, Y. Gofer, U. Heider, R. Oesten, M. Schmidt, J. Electrochem. Soc. 147 (2000) 1322–1331.
[10] K. Edström, T. Gustafsson, J.O. Thomas, Electrochim. Acta 50 (2004) 397–403.

[11] T. Eriksson, A.M. Andersson, A.G. Bishop, C. Gejke, T. Gustafsson, J.O. Thomas, J. Electrochem. Soc. 149 (2002) A69–A78.
[12] S.K. Martha, E. Markevich, V. Burgel, G. Salitra, E. Zinigrad, B. Markovsky, H. Sclar, Z. Pramovich, O. Heik, D. Aurbach, I. Exnar, H. Buqa, T. Drezen, G. Semrau, M. Schmidt, D. Kovacheva, N. Saliyski, J. Power Sources 189 (2009) 288–296.
[13] Y. Talyosef, B. Markovsky, R. Lavi, G. Salitra, D. Aurbach, D. Kovacheva, M. Gorova, E. Zhecheva, R. Stoyanova, J. Electrochem. Soc. 154 (2007) A682–A691.
[14] J. Shim, R. Kostecki, T. Richardson, X. Song, K.A. Striebel, J. Power Sources 112 (2002) 222–230.
[15] D. Aurbach, E. Zinigrad, Y. Cohen, H. Teller, Solid State Ionics 148 (2002) 405–416.
[16] G.G. Amatucci, J.M. Tarascon, L.C. Klein, Solid State Ionics 83 (1996) 167–173.
[17] J. Vetter, P. Novák, M.R. Wagner, C. Veit, K.C. Möller, J.O. Besenhard, M. Winter, M. Wohlfahrt-Mehrens, C. Vogler, A. Hammouche, J. Power Sources 147 (2005) 269–281.
[18] S. Komaba, N. Kumagai, Y. Kataoka, Electrochim. Acta 47 (2002) 1229–1239.
[19] C.H. Chen, J. Liu, K. Amine, J. Power Sources 96 (2001) 321–328.
[20] M.D. Levi, G. Salitra, B. Markovsky, H. Teller, D. Aurbach, U. Heider, L. Heider, J. Electrochem. Soc. 146 (1999) 1279–1289.
[21] C.S. Johnson, N. Li, C. Lefief, J.T. Vaughey, M.M. Thackeray, Chem. Mater. 20 (2008) 6095–6106.
[22] G. Paasch, K. Micka, P. Gersdorf, Electrochim. Acta 38 (1993) 2653–2662.
[23] E. Barsoukov, J.R. Macdonald, Impedance Spectroscopy: Theory, Experiment, and Applications, Wiley-Interscience, 2005.
[24] Q.-C. Zhuang, T. Wei, L.-L. Du, Y.-L. Cui, L. Fang, S.-G. Sun, J. Phys. Chem. C 114 (2010) 8614–8621.
[25] E. Barsoukov, J.H. Kim, J.H. Kim, C.O. Yoon, H. Lee, Solid State Ionics 116 (1999) 249–261.
[26] P. Verma, P. Maire, P. Novák, Electrochim. Acta 55 (2010) 6332–6341.
[27] W. Li, B.L. Lucht, J. Electrochem. Soc. 153 (2006) A1617–A1625.
[28] O. Haik, N. Leifer, Z. Samuk-Fromovich, E. Zinigrad, B. Markovsky, L. Larush, Y. Goffer, G. Goobes, D. Aurbach, J. Electrochem. Soc. 157 (2010) A1099–A1107.
[29] S.K. Martha, H. Sclar, Z. Szmuk Framowitz, D. Kovacheva, N. Saliyski, Y. Gofer, P. Sharon, E. Golik, B. Markovsky, D. Aurbach, J. Power Sources 189 (2009) 248–255.
[30] J. Nanda, J. Remillard, A. O'Neill, D. Bernardi, T. Ro, K.E. Nietering, J.-Y. Go, T.J. Miller, Adv. Funct. Mater. 21 (2011) 3282–3290.
[31] A. Sadezky, H. Muckenhuber, H. Grothe, R. Niessner, U. Pöschl, Carbon 43 (2005) 1731–1742.
[32] F. Amalraj, D. Kovacheva, M. Talianker, L. Zeiri, J. Grinblat, N. Leifer, G. Goobes, B. Markovsky, D. Aurbach, J. Electrochem. Soc. 157 (2010) A1121–A1130.
[33] J. Lei, F. McLarnon, R. Kostecki, J. Phys. Chem. B 109 (2004) 952–957.